SCIENCE CHINA
Earth Sciences

•RESEARCH PAPER•

March 2019 Vol.62 No.3: 571–584
https://doi.org/10.1007/s11430-018-9282-8

Clay mineralogy of an Eocene fluvial-lacustrine sequence in Xining Basin, Northwest China, and its paleoclimatic implications

Bin HU[1,2], Chunxia ZHANG[1,2,3,4*], Haibin WU[1,2,4,5], Qingzhen HAO[1,2,4,5] & Zhengtang GUO[1,2,4,5]

[1] *Key Laboratory of Cenozoic Geology and Environment, Institute of Geology and Geophysics, Chinese Academy of Sciences, Beijing 100029, China;*
[2] *Institution of Earth Science, Chinese Academy of Science, Beijing 100029, China;*
[3] *College of Earth Science and Engineering, Shandong University of Science and Technology, Qingdao 266590, China;*
[4] *CAS Center for Excellence in Life and Paleoenvironment, Beijing 100044, China;*
[5] *University of Chinese Academy of Sciences, Beijing 100049, China*

Received April 8, 2018; revised August 31, 2018; accepted September 28, 2018; published online January 16, 2019

Abstract The Eocene was marked by significant cooling during which the global climate was transformed from greenhouse to icehouse conditions. Notable coeval events were the India-Asia collision and the retreat of the Paratethys Sea in Asia. The Eocene section of the long and continuous sedimentary succession of the Xining Basin in Northwest China is characterized by red mudstones with intercalated gypsum and muddy-gypsiferous layers. In this study, we conducted a semi-quantitative analysis of the mineralogy of bulk samples and the clay fraction using X-ray diffraction, with the aim of characterizing the Eocene climatic evolution of the northeastern margin of the Tibetan Plateau and inland Asia. We used a new pretreatment method to address the problem of extracting sufficient clay particles from the gypsum and gypsiferous layers. The bulk mineralogy is dominated by quartz, feldspar, calcite, gypsum and dolomite; and the clay mineralogy is dominated by illite, chlorite, and smectite (including irregular mixed-layer illite-smectite (I/S)). The variations of the clay mineral assemblages indicate the occurrence of alternations between warm humid conditions and hot dry conditions, with relatively high humidity during ~52–50, ~41.5–39 and ~35–34 Ma. Comparison of the results with the timing of Tibetan Plateau uplift, transgressions and regressions of the Paratethys Sea, and the marine oxygen isotope record suggest that the Eocene climatic evolution of the study region was driven fundamentally by global climate change.

Keywords Eocene, Xining Basin, Clay minerals, Paleoclimate

Citation: Hu B, Zhang C, Wu H, Hao Q, Guo Z. 2019. Clay mineralogy of an Eocene fluvial-lacustrine sequence in Xining Basin, Northwest China, and its paleoclimatic implications. Science China Earth Sciences, 62: 571–584, https://doi.org/10.1007/s11430-018-9282-8

1. Introduction

During the Eocene, the global climate experienced a sustained cooling trend with relatively brief warming events superimposed (Vonhof et al., 2000; Zachos et al., 2008; Bohaty et al., 2009; Lear et al., 2008). There was a global shift from greenhouse conditions, with no polar ice-sheets, to icehouse conditions during the so-called 'doubthouse'; this shift was characterized by climatic cooling, rapid growth of the Antarctic ice sheet, and a supposed decrease in atmospheric carbon dioxide levels, which led to the Eocene Oligocene Transition (EOT) (Eldrett et al., 2009; Pearson et al., 2009). Coeval background events in Asia include the India-Asia collision with associated regional mountain uplift and the retreat of the Tethys Sea, which were likely responsible for monsoon intensification and continental aridification

* Corresponding author (email: cxzhang@mail.iggcas.ac.cn)

(Tang et al., 1992; Beck et al., 1995; Patzelt et al., 1996; Burtman, 2000; Bosboom et al., 2011, 2014b). The Eocene climate of China was dominated by a zonal pattern with a broad W-E arid belt attributable to the planetary circulation system (Liu and Guo, 1997; Sun and Wang, 2005; Guo et al., 2008; Zhang et al., 2012). At this time, northwestern China was located within the broad arid belt and from the early Miocene (22–25 Ma) its climate was transformed to a monsoon-dominated system with 'inland' aridity (Guo et al., 2002, 2008; Sun and Wang, 2005). The origin and evolution of this climatic system has been comprehensively characterized by systematic studies of eolian deposits (Liu et al., 1985; Ding et al., 1999; An et al., 2001; Guo et al., 2002; Qiang et al., 2011; Zhang et al., 2015). However, the origin and evolution of the climate within the arid band, and its driving mechanisms, are comparatively poorly understood due to the lack of long-term continuous terrestrial records.

Most of the early Cenozoic terrestrial records from northwestern China span the late Eocene through early Oligocene (Dupont-Nivet et al., 2008; Pei et al., 2009; Kraatz and Geisler, 2010; Xiao et al., 2010; Abels et al., 2011; Bosboom et al., 2011; Wang et al., 2013; Zhang and Guo, 2014); moreover, there are few long, continuous records of Eocene climate. According to biomarker analysis of the sediments of Xining Basin, the Eocene climate was characterized by progressive aridification with a stepwise pattern of development (Long et al., 2011; Fang et al., 2015). Persistent aridification is also revealed by a sedimentary and pollen record from Lanzhou Basin spanning 51–31.5 Ma (Deng et al., 2010; Yue et al., 2001). However, an alternative view, based on pollen analysis of a sedimentary sequence from Xining (Hoorn et al., 2012) and Jiuquan Basins (Miao et al., 2008), is that the arid trend was punctuated by several relatively humid intervals. In addition, a multi-proxy climate record from Qaidam Basin indicated that the climate was warm and humid during 48.5–40.5 Ma and that temperature and humidity decreased after 40 Ma (Song et al., 2013). Therefore, more high-resolution long-term terrestrial records are needed to better understand the climatic evolution of both northwestern China and the Asian interior during the Eocene.

Xining Basin is located at the transition of three climatic zones: the eastern monsoon zone, western arid zone and Tibetan Plateau zone. The exceptionally long and continuous sedimentary sequence of Xining Basin, consisting of red mudstones with intercalations of gypsum and muddy-gypsiferous layers, provides an excellent opportunity to investigate the origin and evolution of continental aridification in northwestern China (Qinghai Bureau of Geology and Mineral Resources, 1985; Dai et al., 2006; Dupont-Nivet et al., 2007). Comprehensive magnetostratigraphic and palynological investigations have been conducted on the sequence, with previous relatively high-resolution climatic reconstructions focusing on key climatic intervals such as the Middle Eocene Climate Optimum (MECO) and the Eocene-Oligocene Transition (EOT) (Abels et al., 2011; Hoorn et al., 2012; Bosboom et al., 2014a; Zhang and Guo, 2014). However, information on the long-term Eocene climatic evolution in Xining Basin is lacking because of limited pollen recovery from the reddish mudstone beds and the difficulty of extracting clay particles from the gypsum/gypsiferous layers.

Since clay minerals are the products of weathering controlled by climatic and geomorphological factors, variations in their concentration can be used as a climatic proxy (Singer, 1984; Gylesjö and Arnold, 2006). Zhang and Guo (2014) used clay mineralogy and magnetic properties to reconstruct the pattern of climate change during the EOT; in addition, climatic records based on clay mineral assemblages are in agreement with those based on other proxies from sedimentary basins in the Tibet region (Hong et al., 2010; Wang et al., 2011, 2013). Thus, the Eocene climatic evolution of the Xining Basin can potentially be reconstructed by clay minerals assemblages.

In this study, we developed a new pretreatment method to address the problem of extracting clay particles from gypsum and gypsiferous layers (Hu et al., 2016), and used it to reconstruct the Eocene climatic evolution of Xining Basin based on clay and bulk mineralogical analyses. Our results provide additional evidence for the nature of early Cenozoic climate change in the northeastern Tibetan Plateau and inland Asia.

2. Materials and methods

2.1 Geographical and geological setting

Xining Basin is located in the northeastern margin of the Tibetan Plateau (from 36°00′–37°15′N and from 101°00′–103°00′E) and the elevation ranges from ~2250–3000 m. Today, it is dominated by a semi-arid continental climate with annual average temperature ranging from 4.9–7.1°C and annual precipitation from ~243.2–564 mm. During summer, the region experiences high temperatures accompanied by high precipitation, reflecting the influence of the East Asian monsoon.

Xining Basin is a Mesozoic-Cenozoic clastic depocenter structurally controlled by two sinistral transpressional faults (the middle Qilian Shan Fault in the north and the Laji Shan Fault in the south) and a secondary fault (Datong Fault) (Figure 1). Deposition within the basin commenced at ~52 Ma (Dai et al., 2006). The Cenozoic sedimentary successions in Xining Basin lie disconformably on Mesozoic alluvial sediments of the Hekou and Minhe Groups (possibly of lower and upper Cretaceous age, respectively) or disconformably on Cretaceous basement rocks. The Cenozoic saline lake to fluvio-lacustrine sedimentary succession is

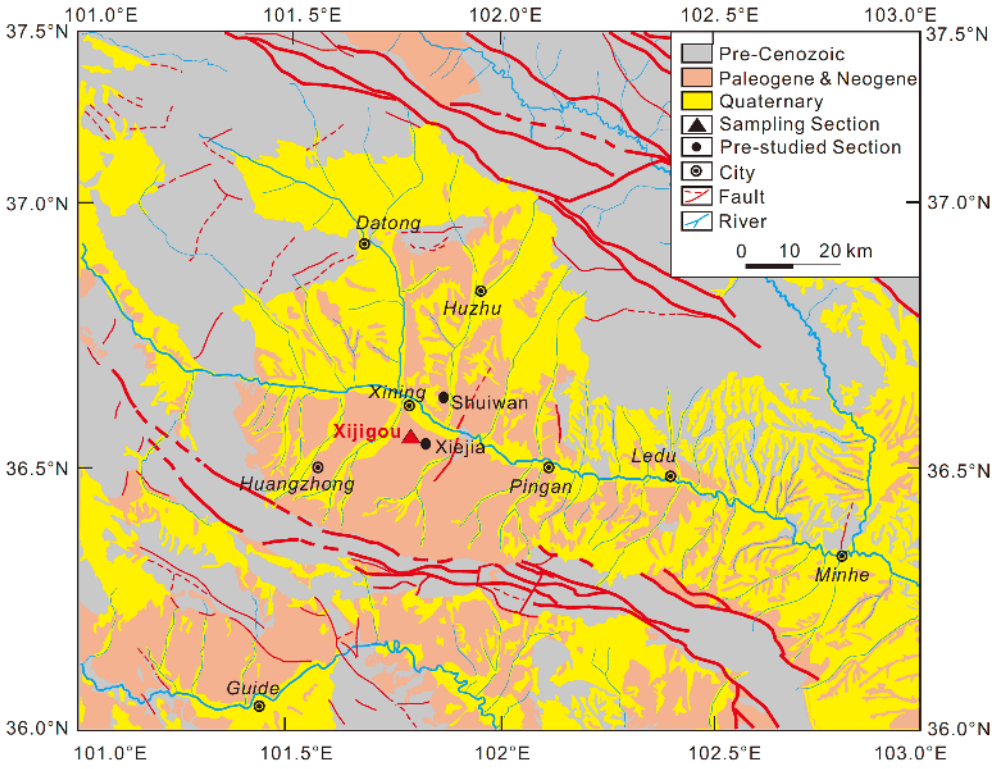

Figure 1 Geological map of the vicinity of the Xijigou section. Modified after Xiao (2009).

divided into the Xining and Guide Groups. The Xining Group is subdivided into the Qijiachuan Formation (Paleocene to possibly Early Eocene), the Honggou Formation (Early-mid Eocene), and the Mahalagou Formation (Late Eocene-Oligocene). The Xining Group is disconformably overlain by the Guide Group (Dai et al., 2006).

In this study, we focus on the Tertiary interval from the Honggou Formation to the Mahalagou Formation in the Xijigou section (Figure 2); the section is located in the central southern part of Xining Basin, 7 km from Xining city, and is 448 m thick. The Honggou Formation developed during ~52–41.5 Ma (Dai et al., 2006) and is characterized by reddish mudstone. Since the lithology is relatively uniform, the ages can be estimated from the mean sedimentation rate. The Mahalagou Formation overlies the Honggou Formation, and the termination of a very thick gypsum layer at the top of the section (420 m depth) is dated to ~34 Ma (Dai et al., 2006; Xiao, 2009; Zhang and Guo, 2014). The Mahalagou Formation can be divided into three intervals based on distinctive lithologies: a gypsum-rich lower interval (~41.5–37 Ma), a mudstone-rich middle interval (~37–34 Ma), and an upper interval which consists exclusively of mudstone and in which gypsum is absent (~34–31 Ma) (Dai et al., 2006; Dupont-Nivet et al., 2007; Abels et al., 2011). In the studied section of the Mahalagou Formation, the gypsum-rich and mudstone-rich intervals are within the depth intervals of 157–295 and 295–420 m, respectively (Figure 2). The gypsum-rich interval consists of laminated gypsum alternating with mudstone from 157–202 m (~41.5–39 Ma) and massive gypsum layers from 202–295 m (~39–37 Ma) (the chronology is based on Abels et al., 2011). For the present study, we collected a total of 130 samples, at a 3 m interval, for mineralogical analyses of the bulk and clay fractions.

2.2 Measurements of the mineralogy of bulk samples and the clay fraction

Analysis of bulk samples can be used to identify and semi-quantify the mineral composition of different layers, and when combined with lithology it can be used to characterize changes in sedimentary facies within a region. Clay mineral analysis is used to identify and semi-quantify the composition of clay particles. The bulk fraction and clay fraction (<2 μm) of all samples were analyzed using X-ray diffraction (XRD), conducted with a PANalytical diffractometer with Ni-filtered Cu-Kα radiation (40 kV, 40 mA) at the Laboratory of Soil Structure and Mineralogy, Institute of Geology and Geophysics, Chinese Academy of Sciences.

Bulk samples were ground to <45 μm with an agate mortar and then packed into the groove of a glass sample holder, producing a flat surface. For the bulk samples, XRD measurements were made using a step size of 0.020° 2θ and a scan rate of 0.020° 2θ s^{-1}, from 2° 2θ to 35° 2θ. Identification of bulk minerals was based on the positions of the following peaks: gypsum, 7.60 A; quartz, 4.26 A; feldspars, 3.18 A;

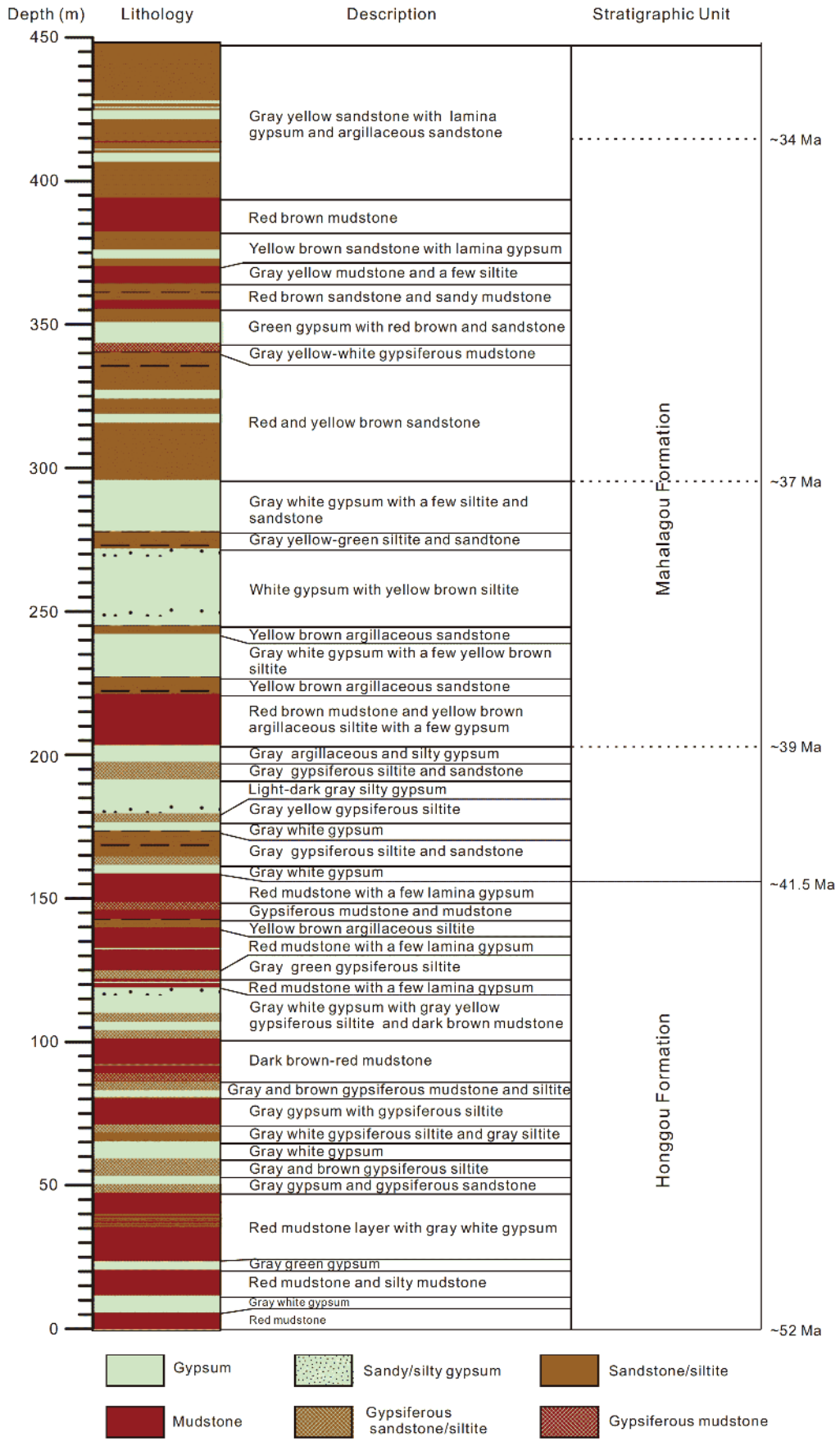

Figure 2 Lithology and stratigraphy of the Xijigou section.

calcite, 3.04 A; and dolomite, 2.89 A (Figure 3c). Bulk mineral abundances were determined using Highscore software, provided by PANalytical B.V.

Two different pretreatment methods were used to extract the clay fraction (<2 μm). The samples used were mainly from mudstone/siltstone/sandstone and from gypsum layers. For mudstone/siltstone/sandstone, we used the standard pretreatment method (Zhang and Guo, 2014); however, this method is less effective for extracting clay particles from gypsum layers. To address this problem, we modified the method by introducing treatment with an EDTA (disodium ethylenediaminetetraacetic acid) solution which resulted in a substantial increase in the quantity of clay particles extracted from gypsum-rich samples (Hu et al., 2016).

The clay fraction (<2 μm) obtained using the standard and modified pretreatment methods was saturated with $MgCl_2$ and KCl, respectively. The $MgCl_2$ replaces the cations within the interlayers of the clay minerals, thus reducing d-spacing variability (Moore and Reynolds, 1989). To identify the expansion minerals, we divided the $MgCl_2$-saturated sample into two parts, to each of which glycerol and ethylene glycol were added respectively. To distinguish kaolinite from chlorite, we heated the KCl-saturated samples to 300 and 550°C. The procedure for XRD analysis of the clay minerals followed the methods described in detail by Zhang and Guo (2014). XRD analysis of the clay minerals was performed using a step size of 0.020° 2θ and a scan rate of 0.050° 2θ s^{-1}, from 3° 2θ to 30° 2θ. Identification of clay minerals was based on the position within XRD diagrams of the (001) series of basal reflections in eight different sample splits: air-dry (AD: original, Mg-saturated and K-saturated); Mg-saturated with ethylene glycol (EG) and glycerol (G); and K-saturated and heated to 300 and 550°C (Figure 3a and 3b). Semi-quantification of clay minerals was carried out on the glycerol curve using MacDiff software (Petschick, 2000). The procedures are described in detail in Zhang and Guo (2014).

3. Results

3.1 Bulk sample mineralogy

The bulk samples are mainly composed of gypsum, quartz, feldspar, calcite and dolomite (Figure 3c). The distribution of the bulk mineral assemblages is plotted versus depth/age in Figure 4. The concentration ranges of the major minerals are summarized as follows: Gypsum ranges from 1–99% (median 73%). The carbonate minerals comprise calcite and dolomite, with dolomite ranging from 1–81% (median 4%) and calcite from 1–22% (median 4%). Quartz ranges from 1–18% (median 6%); feldspar from 1–31% (median 3%); and the concentration of clay particles from 0–55% (median of 4%). Three zones (Zones A–C) can be recognized based on the variations in lithology and mineralogy of the bulk samples, with boundaries at the depths of 226 and 298 m. In Zone A (0–226 m, ~52–39 Ma), the concentrations of gypsum, quartz, feldspar and clay exhibit large amplitude fluctuations; in addition, there is an increase in gypsum and decreases in quartz, feldspar and clay. In Zone B (226–298 m, ~39–37 Ma), gypsum is the dominant mineral and the calcite concentration is the highest among the three zones; the concentrations of dolomite quartz, feldspar and clay decrease abruptly, mirroring the high gypsum concentration. In Zone C (298–448 m, basal age ~37 Ma), the concentrations of quartz, feldspar and clay increase and those of calcite and gypsum decrease.

3.2 Clay fraction mineralogy

The clay mineral assemblages of the Xijigou section are mainly composed of illite, chlorite and smectite (including irregular mixed-layer illite-smectite (I/S)) with a small quantity of quartz and feldspar (Figure 3a and 3b). As shown in Table 1, illite is the dominant clay mineral, ranging from 62–97% (median 87%). Chlorite is less abundant, ranging from 2–20% (median 9%). Smectite (including I/S) ranges from 0–28% (median 2%). The concentrations of smectite (including I/S), illite and chlorite in gypsum/gypsiferous layers are similar to those of the red mudstones (Table 1).

The clay mineral concentrations are plotted versus depth/formation in Figure 5. Based on the variation of smectite (including I/S) content, three sub-zones can be defined within Zone A (Zone A-1 to Zone A-3). The age of the top of Zone A-1 is estimated at ~50 Ma based on the mean sedimentation rate; the top of Zone A-2 corresponds to the boundary between the Honggou and Mahalagou Formations (157 m depth, ~41.5 Ma); and Zone A-3 ranges from 157–226 m depth. Zones B and Zone C are identical to those defined from the bulk sample mineralogy. The variations of the lithology and clay mineral content within Zone C are identical to those described in previous research of the EOT in Xining Basin (Zhang and Guo, 2014). According to Zhang and Guo (2014), the ages of the interval of high smectite content (including I/S) (355–415 m depth) within Zone C range from ~35–34 Ma. The clay mineral characteristics of the three zones are described as follows:

Subzone A-1 (0–39 m, ~52–51 Ma), the concentration of smectite (including I/S) decreases gradually from 23% to near zero at the end, while that of chlorite increases from 3–17%.

Subzone A-2 (39–157 m, ~51–41.5 Ma), the smectite content (including I/S) is low and uniform, ranging from 0–9%; in addition, the illite content is relatively high and uniform, ranging from 80–97%.

Subzone A-3 (157–226 m, ~41.5–39 Ma), the smectite content (including I/S) increases to 26.3%, and the illite

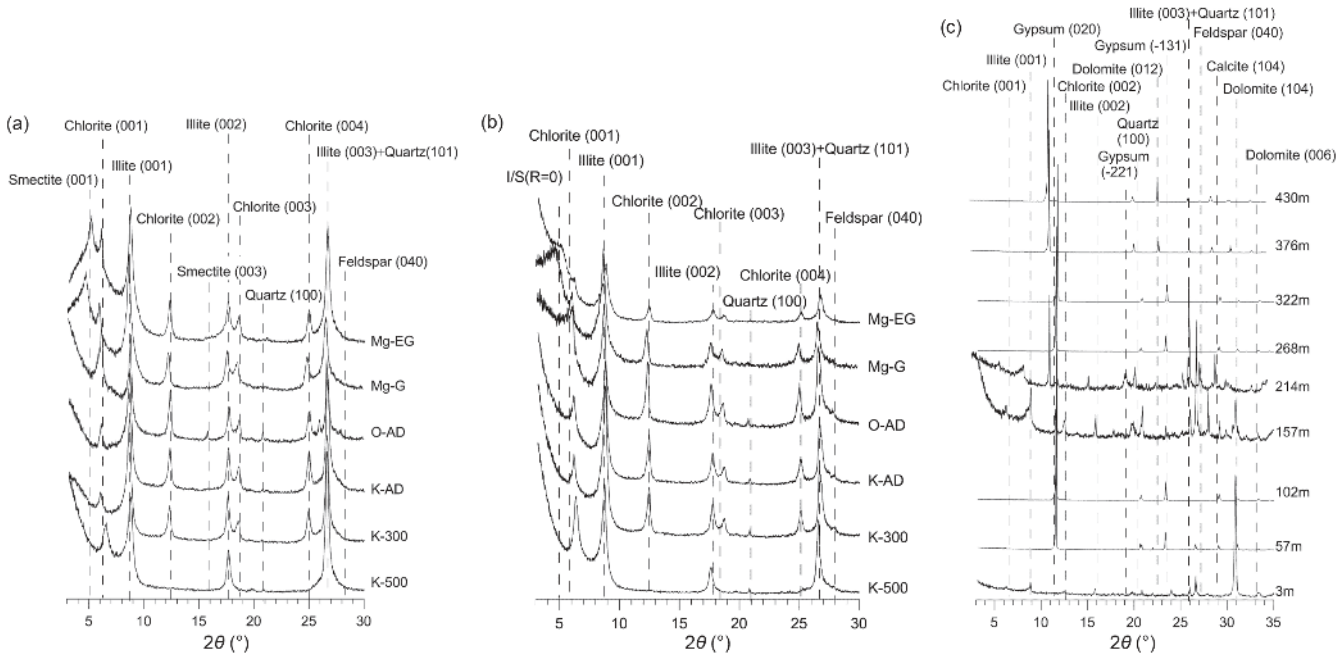

Figure 3 X-ray diffractograms of typical clay mineral and bulk samples. (a) Siltstone sample using the conventional pretreatment method, containing illite, chlorite and I/S (R=0). (O-AD, Original sample; Mg-EG, Mg-saturated with ethylene glycol; Mg-G, Mg-saturated with glycerol; K-AD, K-saturated without heating; K-300, K-saturated with heating at 300°C; K-500, K-saturated with heating at 500°C). (b) Gypsum sample pretreated with EDTA solution, containing illite, chlorite and smectite. (c) Bulk samples from different depths of the Xijigou section.

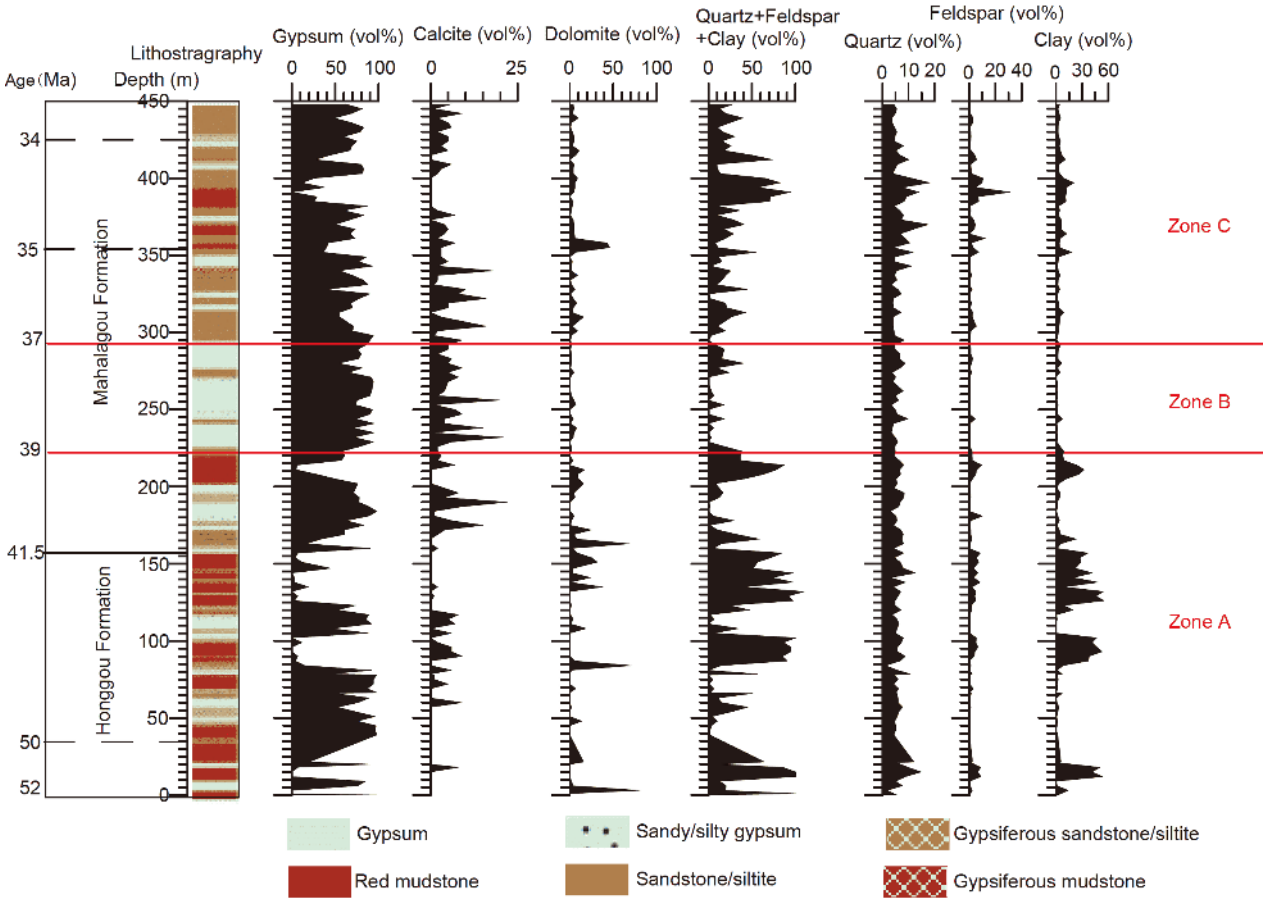

Figure 4 Lithology and bulk sample mineralogical composition of the Xijigou section.

Table 1 Summary of the clay mineral composition of the major lithologies of the Xijigou section

Mineral		All samples	Red mudstone	Gypsum/Gypsiferous
Sample No.		(130)	(101)	(29)
(I/S+Sm)(%)	Range	0–28	0–28	0–16
	Median	2	3	0
I(%)	Range	62–97	62–97	79–96
	Median	87	86	89
Ch(%)	Range	2–20	2–20	4–18
	Median	9	9	10

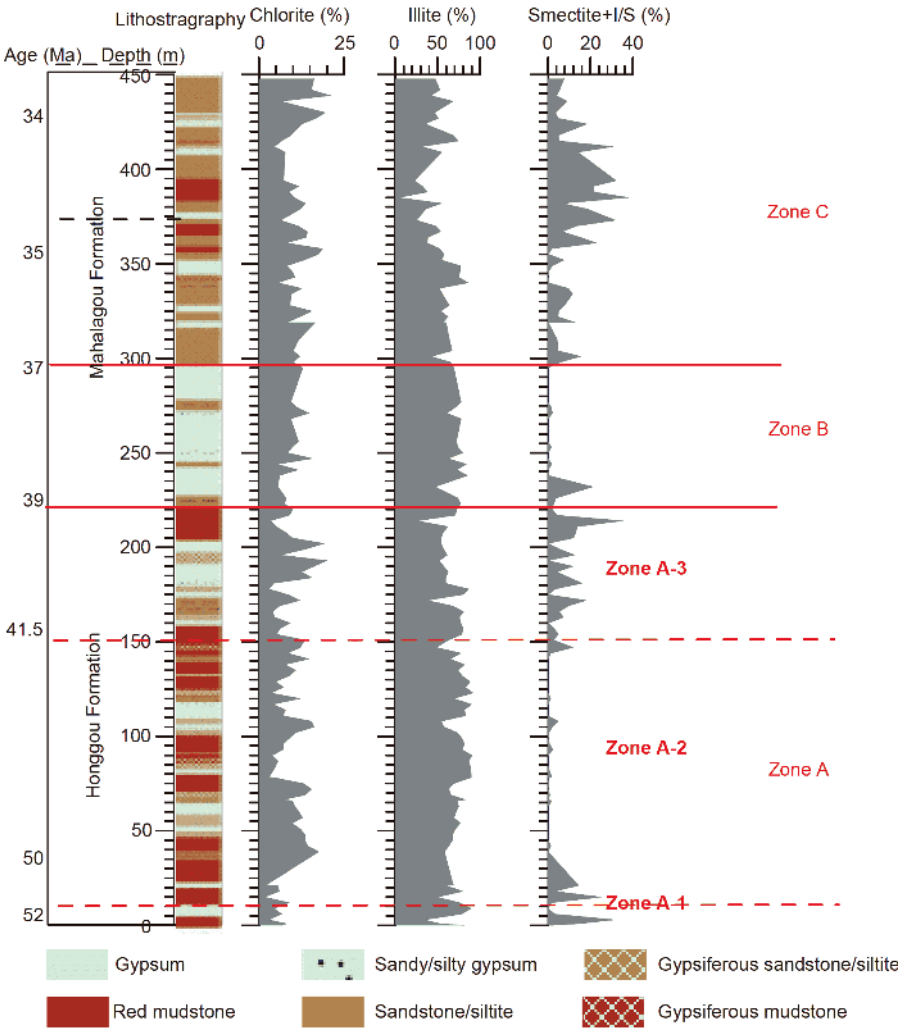

Figure 5 Lithology and clay mineral composition of the Xijigou section.

content decreases to 70%.

Zone B (226–298 m, 39–37 Ma), the smectite content (including I/S) decreases rapidly and ranges from 0–2%; the illite content remains high, ranging from 79–94%; and the chlorite content increases gradually from 5–15%.

Zone C (298–448 m, 37–34 Ma), the smectite content (including I/S) increases from the base to 28% and then decreases to 6%. There is an interval of high smectite abundance (including I/S) from 355–415 m. Illite and chlorite exhibit inverse trends of variation to smectite (including I/S), first decreasing and then increasing; their lowest levels occur within the interval of 355–415 m.

4. Discussion

4.1 Formation of clay minerals and their climatic significance

Most of the clay minerals in soils are produced by weath-

ering of the underling parent rocks and sediments. Hence, variations in the composition and concentration of clay minerals within sedimentary sequences can reflect climatic fluctuations within the surrounding area. In the initial stage of weathering, muscovite can be hydrolyzed to illite, and then as weathering progresses illite can be transformed to smectite; in a tropical climate, smectite can subsequently (with the elution of K^+) be transformed to kaolinite and gibbsite (Chamley, 1989; Velde, 1995). Illite and chlorite are the main products of physical weathering under a cold/dry climate (Velde, 1995). In regions of low relief and warm climate, smectite forms with seasonal alternations of humid and dry conditions: water logging occurs during the humid season and during the following dry season the soil solutions become concentrated (Robert and Kennett, 1994). Vermiculite and mixed-layer clays are indicative of humid conditions, and kaolinite and gibbsite are the final products of hydrolysis and leaching of metal ions under a hot and wet climate (Velde, 1995).

In Xining Basin there are no differences in clay mineral assemblages between gypsum/gypsiferous layers and the mudstone beds, which are dominated by illite, chlorite and smectite (including I/S). The clay mineral concentrations vary with depth (Figure 5) and a notable characteristic is that the concentrations of smectite (including I/S) fluctuates inversely with that of illite. No major regional tectonic event occurred in Xining Basin during 52–34 Ma (Dai et al., 2006); in addition, zircon U-Pb age spectra and paleocurrent directions indicate that the sedimentary provenance of Xining Basin was stable during ~52–34 Ma, with the sediments derived from Triassic flysch sediments of the eastern Kunlun Shan, western Qinling and Qilian Shan (Zhang et al., 2016). Therefore, the variations of the clay mineral concentration of the study section are likely to reflect climate change with the minimal influence of tectonic activity.

A previous clay mineral investigation of the EOT of Xining Basin (Zhang and Guo, 2014) proposed that the environment responsible for the formation and preservation of smectite within the catchment of Xining Basin was characterized by alternating warm and humid and hot and dry conditions. As mentioned above, illite and chlorite are produced by physical weathering under a cold or dry climate. The absence of kaolinite, and the dominance of illite and chlorite, in the sediments of Xining Basin imply an arid climatic background with relatively low intensity chemical weathering. Therefore, the proportion of smectite (including I/S) can be interpreted as a humidity index and the proportion of chlorite and illite as an aridity index.

4.2 Eocene climate of Xining Basin inferred from the clay mineral record

To characterize the climatic variations recorded by the studied section we used the following index: (smectite+I/S)/(chlorite+illite)), abbreviated to (Sm+I/S)/(Ch+Ill); high values of the ratio indicate relatively wet conditions and low values indicate relatively dry conditions. We also compared the depth variation of the ratio with that a complementary index, the Chemical Index of Weathering (CIW'), from Xining Basin (Sayem et al., 2018).

Depth profiles of (Sm+I/S)/(Ch+Ill) ratio and CIW' are illustrated in Figure 6a and 6b. The two indexes co-vary and they indicate the occurrence of regional humidity variations against an overall arid climatic background. During ~52–50 Ma, the intensity of chemical weathering, hence humidity, was relatively high. During ~50–41.5 Ma, the reduced intensity of chemical weathering and lower humidity indicated by the clay mineral ratios suggests that the climate became drier. During ~41.5–39 Ma, the intensity of chemical weathering and humidity increased again, indicating the return of relatively warm conditions. During ~39–37 Ma, a lower intensity of chemical weathering and reduced humidity suggest that the climate became drier. After ~37 Ma, there was a third phase of increased chemical weathering and humidity, with maximum humidity during ~35–34 Ma. Finally, after ~34 Ma, the intensity of chemical weathering and humidity decreased for the third time. These changes clearly demonstrate that the Eocene climate of Xining Basin was characterized by alternating between warm humid and hot dry conditions. Although there are substantial fluctuations in both (Sm+I/S)/(Ch+Ill) and CIW', there is a long-term decrease in CIW', which is not evident in (Sm+I/S)/(Ch+Ill), and implies the gradual intensification of aridification in Xining Basin. The contrast between the two indexes suggests that while clay minerals are sensitive indicators of warming events, long-term climatic trends in arid regions may need to be identified using other indexes.

Palynological studies of Xining Basin provide valuable independent information about Eocene climatic evolution, A tropical-subtropical hot and humid climate occurred during ~52–50 Ma, and a cooler and drier climate during ~50–42 Ma (Chen, 2009). During ~42–40 Ma, the climate was warm and wet and then became arid during ~40–38 Ma, indicated by an increase in desert-steppe taxa and a decrease in broadleaved forest taxa (Figure 6c and 6d; Bosboom et al., 2014a). During 39.9–36.4 Ma, the climate was warm and wet and then became cooler and drier during 36.4–33.5 Ma, based on an abrupt increase in the representation of conifers and the disappearance of broadleaved forest taxa (Hoorn et al., 2012; Figure 6c). Our climatic reconstruction based on clay mineral analysis is very similar to the conclusions based on palynological research, except for the interval of ~36.4–33.5 Ma. During this interval, a peak in conifer representation and decrease in xerophilous taxa was interpreted by Hoorn et al. (2012) as reflecting a cooler and drier climate;

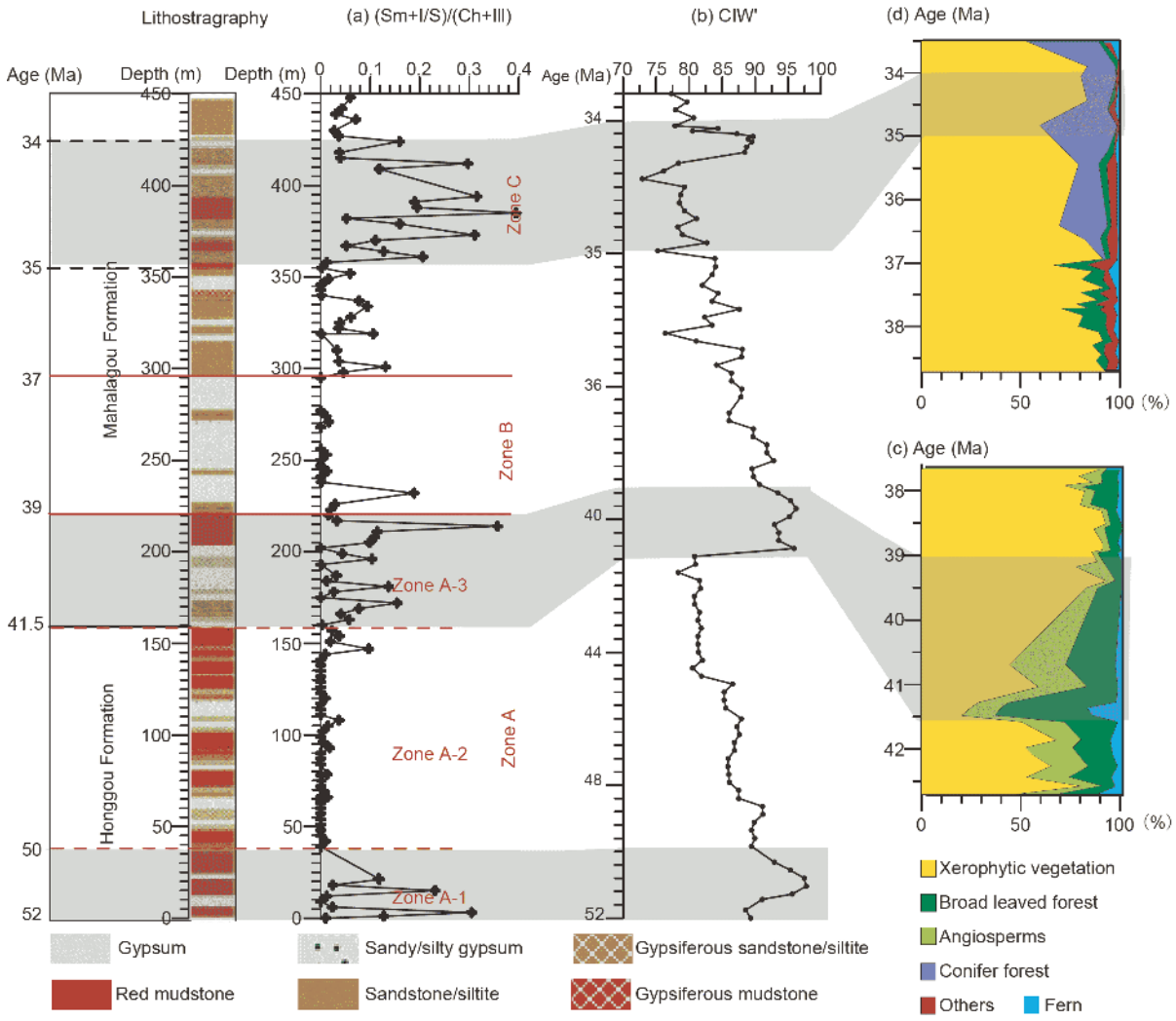

Figure 6 (a) Lithology and variation of the (Sm+I/S)/(Ch+Ill) ratio for the Xijigou section. (b) Variation of the Chemical Index of Weathering (CIW') in Xining Basin (from Sayem et al., 2018). (c) Summary pollen diagram spanning ~42–38 Ma from Xining Basin (modified from Bosboom et al., 2014a). (d) Summary pollen diagram spanning ~38.5–35.5 Ma from Xining Basin (modified from Hoorn et al., 2012).

however, the (Sm+I/S)/(Ch+Ill) ratio indicates higher humidity. Previous research has shown that relatively high humidity is needed for the growth of coniferous vegetation (annual mean relative humidity of 70–80%; Chen, 2009). Therefore, coniferous vegetation is predominantly an indicator of a cool and wet climate (Shi et al., 1996; Zhang et al., 2006), which is compatible with the results of our clay mineral analysis. However, the overall consistency between the palynological and clay mineral records for Xining Basin validates our clay mineral-based Eocene climatic reconstruction for the region.

In summary, the results of clay mineral analysis reveal that the Eocene climate of Xining Basin was characterized by alternations between warm humid and hot dry conditions, with relatively high humidity during ~52–50, ~41.5–39 and ~35–34 Ma, and arid conditions during ~50–41.5 and ~39–37 Ma.

4.3 Potential drivers of the Eocene climatic evolution of Xining Basin

The overall arid climate of Xining Basin during the Eocene was determined predominantly by the broad W-E arid belt attributable to the planetary circulation system (Liu and Guo, 1997; Sun and Wang, 2005; Guo et al., 2008; Zhang et al., 2012). However, possible causes of the fluctuations in humidity indicated by variations in the (Sm+I/S)/(Ch+Ill) ratio are: the uplift of the Tibetan Plateau, transgressions and regressions of the Paratethys Sea, and global climate change. We now assess each of these potential drivers.

4.3.1 Tibetan Plateau uplift

The Cenozoic uplift of the Tibetan Plateau, initiated by the India-Asia collision, had a profound impact on the Asian environment and on global climate change. Although the timing of the initiation of the India-Asia collision is still

debated, the bulk of the evidence suggests that it probably occurred between the late Cretaceous and the Eocene (55±10 Ma) (Ding et al., 2005; Najman et al., 2010; Cai et al., 2011; Lippert et al., 2014). Thus, most of the Tibetan Plateau uplift postdated 55±10 Ma. Abundant evidence of a transition from marine to terrestrial successions reveals that most of the area of the modern Tibetan Plateau was close to or above sea-level until 45–40 Ma (Rowley, 1996; Wang et al., 2002; Zhu et al., 2005). Only the Gangdese Mountains and Lhasa terrane in the south, and the Qiangtang terrane in the centre of the region, had been uplifted to a relatively high altitude (Hetzel et al., 2011; Rohrmann et al., 2012; Wang et al., 2008; Rowley and Currie, 2006; Xu et al., 2013). According to palynological records from Hoh Xil Basin in the northern Tibetan Plateau, the paleoelevation was relatively low (<2000 m); in addition, palynological records from the adjacent basins, including the Qaidam, Xining and Lanzhou Basins (Miao et al., 2016), are similar to that of Hoh Xil Basin. Thus, we infer that the paleoelevation of Xining Basin in the late Eocene was still relatively low and that the influence of Tibetan Plateau uplift was limited to the region distal to the northeastern margin. Therefore, it is likely that the climatic conditions reflected by the (Sm+I/S)/(Ch+Ill) ratio were not determined by the uplift of the Tibetan Plateau uplift prior to 40–37 Ma.

There was a significant increase in coniferous vegetation in Xining Basin during 37–36 Ma which is likely to reflect the altitudinal gradient of the surrounding topography (Dupont-Nivet et al., 2008; Hoorn et al., 2012). However, the sediment accumulation rates in Xining Basin remained stable at 1.8 cm kyr^{-1}, increasing to 4.1 cm kyr^{-1} at 34.5 Ma (Dai et al., 2006). Compared with the substantially higher sediment accumulation rates (20–200 cm kyr^{-1}) in basins in the northern Tibetan Plateau during the Miocene, the slight increase in accumulation rate in Xining Basin suggests that the impact of tectonic uplift was minor and comparatively distal in its effect at 34.5 Ma. Our clay mineral data indicate no increases in the concentrations of illite and chlorite during the late Eocene, and thus there is no evidence for significantly increased physical weathering. On the contrary, the concentrations of smectite (including I/S) increased substantially, suggesting the intensification of chemical weathering. Thus we speculate that the uplift of the northern Tibetan Plateau during 37–34 Ma had little influence on the climate in Xining Basin; moreover, uplift cannot explain the multiple shifts to more humid conditions.

4.3.2 Transgression and regression of the Paratethys Sea

Paleogeographic research indicates that during the early Cenozoic a shallow epicontinental sea extended across Eurasia from the Mediterranean Tethys to the Tarim Basin in western China. This shallow sea underwent multiple transgressions and regressions before becoming ultimately isolated as the Paratethys Sea during the latest Eocene or early Oligocene (Tang et al., 1992; Burtman, 2000; Bosboom et al., 2014b). Climate modelling studies as well as geological evidence show that the retreat of the Paratethys Sea from Central Asia led to aridification and the intensification of the Asian monsoon system and its enhancement as a moisture source for the Asian interior (Ruddiman and Kutzbach, 1989; Prell and Kutzbach, 1992; Sun and Wang, 2005; Kent-Corson et al., 2009; Bosboom et al., 2014b). To explore the linkage between climatic variations and the retreat of the Paratethys Sea, we compared the variation of the (Sm+I/S)/(Ch+Ill) ratio (Figure 7b) and CIW' (Figure 7c) with the transgressions and regressions of the Paratethys Sea in the Tarim Basin (Figure 7a). The occurrence of a relatively high humid climate during ~52–50 Ma is consistent with a contemporaneous transgression of the Paratethys Sea; however, during ~41.5–39 and ~35–34 Ma, the relatively humid climate corresponds to its regression. Therefore, as a potential moisture source, transgressions and regressions of the Paratethys Sea do not correspond to the changes in humidity indicated by the clay mineral record of Xining Basin. In contrast, as previous research on the moisture supply to inland Asia during the Eocene suggested that the dominant influence was the combined effect of the subtropical high and the westerlies, the moisture was mainly from the Paratethys Sea (Caves et al., 2015; Bougeois et al., 2018). Southerly-sourced moisture from the Indian Ocean was continuously blocked and was unable to penetrate northwards reflected a critical altitude of the Tibetan Plateau had been attained. Thus, the westerly-sourced moisture was maintained and it remained the dominant moisture source from at least the early Eocene (Caves et al., 2015). All of this evidence indicates that transgressions and regressions of the Paratethys Sea were not the main driver of the observed climatic variations in Xining Basin during the Eocene.

4.3.3 Influence of global climate change on the Eocene climate of Xining Basin

We compared the variation of the (Sm+I/S)/(Ch+Ill) ratio with the marine oxygen isotope record (Zachos et al., 2001) (Figure 7a and 7f). Notably, the intervals of high humidity during Zone A-1, Zone A-3 and Zone C, are coincident with three warming intervals at ~52–50, ~41.5–39 and ~35–34 Ma, which punctuate a long-term cooling trend evident in the marine oxygen isotope record; in addition, the intervals of increased aridity during Zone A-2 and Zone B are consistent with the cool episodes in the marine oxygen isotope at ~50–41.5 and ~39–37 Ma.

The first warming interval evident in the marine oxygen isotope record at ~52–50 Ma is part of the Early Eocene Climate Optimum (EECO), when the global climate experienced an extreme warming episode across all latitudes during 59–51 Ma, with the warmest stage of the EECO

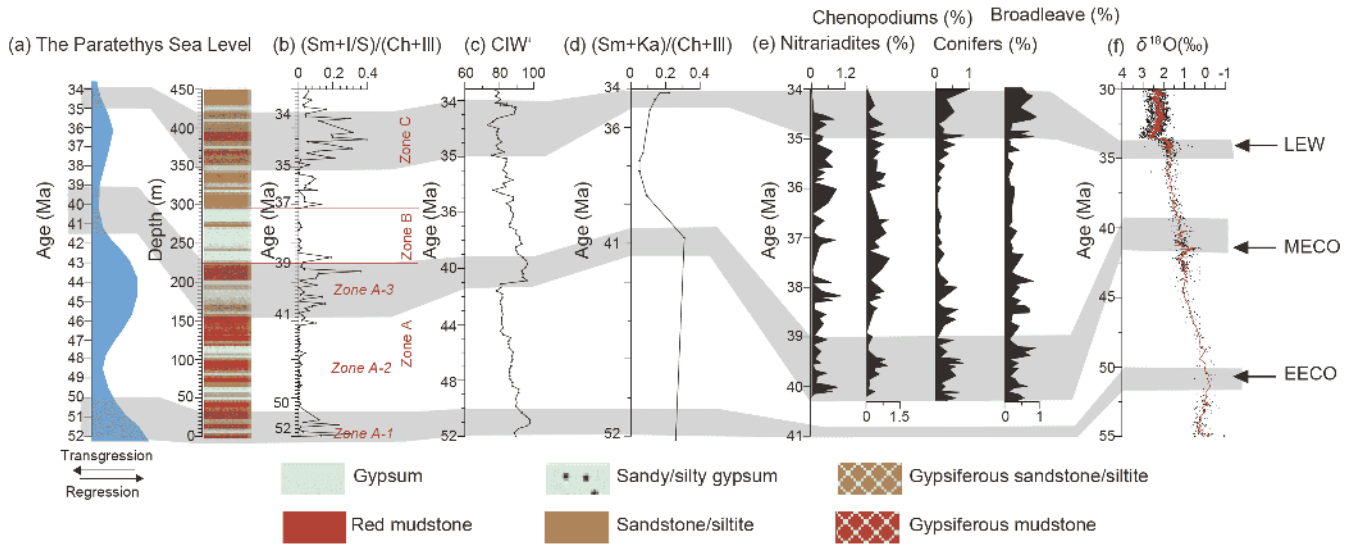

Figure 7 (a) Incursions of the Paratethys Sea into the Tarim Basin (modified from Bosboom et al., 2014b); (b) record of the (Sm+I/S)/(Ch+Ill) ratio of the Xijigou section; (c) record of the Chemical Index of Weathering (CIW') for Xining Basin (from Sayem et al., 2018); (d) record of the (Sm+Kao)/(Ch+Ill) ratio of the Tarim Basin (Ka: kaolinite) (from Wang et al., 2013); (e) palynological record for Jiuquan Basin (from Miao et al., 2008); (f) marine oxygen isotope record (from Zachos et al., 2001).

during 52–50 Ma (Bains et al., 1999; Lear et al., 2000; Zachos et al., 2001, 2003, 2005). Thus the relatively humid interval during ~52–50 Ma in Xining Basin revealed by the clay mineral record is consistent with global climate change. The subsequent cooling after ~50 Ma which lasted to the early Middle Eocene (Lear et al., 2000; Zachos et al., 2001) coincided with an intensification of aridification in Xining Basin revealed by the clay mineral record.

The second warming interval evident in the marine oxygen isotope record during ~41.5–40 Ma is termed the Middle Eocene Climate Optimum (MECO), which is recognized as a warming event of ~500-kyr duration, from ~41.5 to ~40 Ma. It is characterized by gradual warming, then by an abrupt peak in warmth, and then by relatively rapid post-MECO cooling within ~50 kyr (Bohaty et al., 2009; Edgar et al., 2010). The relatively high humidity from ~41.5–39 Ma indicated by the clay mineral record of Xining Basin coincides with the MECO, while the abrupt decrease in humidity during ~39–37 Ma indicated by the clay mineral record was likely a response to the post-MECO cooling event (Bohaty et al., 2009; Edgar et al., 2010).

The third warming interval evident in the marine oxygen isotope record is at ~35–34 Ma. Contemporary Northern Hemisphere continental records from latitudes similar to the Xining Basin indicate a temperature increase of ~2–3°C in Northern Europe and a ~4°C increase in MAT in central North America; this episode is termed the Late Eocene Warming (LEW) (Zachos et al., 2001; Zanazzi et al., 2007; Lear et al., 2008; Hren et al., 2013). The variation of the (Sm+I/S)/(Ch+Ill) record of Xining Basin suggests a rapid increase in humidity which reached a maximum during ~37–34 Ma, followed by a decrease at ~34 Ma. This trend is consistent with the climatic reconstruction of Zhang and Guo (2014) and indicates that a cold and dry climate was sustained until ~33.1 Ma.

The influence of global climate change on inland Asia during the Eocene was not limited to Xining Basin: it is also evident in a clay mineral record from Tarim Basin (Figure 7d; Wang et al., 2013) and in a palynological record from Jiuquan Basin (Figure 7e; Miao et al., 2008). The three intervals of relatively high humidity indicated by our clay mineral record (~52–50, ~41.5–39 and ~35–34 Ma) are consistent with increases in the (Sm+Ka)/(Ch+Ill) ratio in Tarim Basin, as well with an increase in broadleaved forest and decrease in Nitrariadites and Chenopodiums in Jiuquan Basin. Thus, the three humidity intervals in Xining Basin were also recorded in other western basins.

In summary, the three intervals of relatively high humidity in Xining Basin, at ~52–50, ~41.5–39 and ~35–34 Ma, are coeval with the EECO, the MECO and the LEW; while the intervals of increased aridity, during ~50–41.5 and ~39–37 Ma, and up to ~34 Ma, are consistent with cooling intervals evident in the marine oxygen isotope record. Therefore, we conclude that the Eocene climate of Xining Basin was fundamentally driven by global climate change.

5. Conclusions

In this study, we have used XRD to identify and semi-quantify the mineralogy of bulk samples and clay fraction of a sedimentary sequence in Xining Basin, with the aim of characterizing the Eocene climatic evolution of the region. The following principal conclusions can be drawn.

(1) The bulk sample mineralogy is dominated by quartz, feldspar, calcite, gypsum and dolomite; and the clay fraction mineralogy is dominated by illite, chlorite, smectite (including irregular mixed-layer illite-smectite (I/S)). The mineralogical characteristics indicate an overall arid climate in Xining Basin and that the clay mineral assemblages were climatically controlled.

(2) The mineralogical results suggest that the Eocene climate of Xining Basin experienced three fluctuations between warm humid conditions and hot dry conditions, with relatively higher humidity during ~52–50, ~41.5–39 and ~37–34 Ma, and intervals of intensified aridity during ~50–41.5 and ~39–37 Ma.

(3) Comparison with the timing of the uplift of the Tibetan Plateau, transgressions and regressions of the Paratethys Sea, and the marine oxygen isotope record suggests that the Eocene climate of Xining Basin was fundamentally determined by global climate change, and that the three humid intervals in Xining Basin are correlative with the EECO, MECO and LEW.

Acknowledgements *We thank Dr. Pei Li, Dr. Yating Lin, Xiangbing Ren and Shuya Zhu for their help with field work. We also thank Dr. Abu Sayem, Dr. Wenling An and Dr. Xinbo Gao for their valuable suggestions during this study. This work was supported by the National Natural Science Foundation of China (Grant Nos. 41722206, 41430531, 41690114 & 41374072), the Strategic Priority Research Program of the Chinese Academy of Sciences (Grant No. XDB26000000) and the International Cooperation Program of the Chinese Academy of Sciences (Grant No. 131C11KYSB20160061).*

References

Abels H A, Dupont-Nivet G, Xiao G, Bosboom R, Krijgsman W. 2011. Step-wise change of Asian interior climate preceding the Eocene-Oligocene transition (EOT). Palaeogeogr Palaeoclimatol Palaeoecol, 299: 399–412

An Z S, Kutzbach J E, Prell S C. 2001. Evolution of Asian monsoons and phased uplift of the Himalaya-Tibetan plateau since Late Miocene times. Nature, 411: 62–66

Bains S, Corfield R M, Norris R D. 1999. Mechanisms of climate warming at the end of the Paleocene. Science, 285: 724–727

Beck R A, Burbank D W, Sercombe W J, Riley G W, Barndt J K, Berry J R, Afzal J, Khan A M, Jurgen H, Metje J, Cheema A, Shafique N A, Lawrence R D, Khan M A. 1995. Stratigraphic evidence for an early collision between northwest India and Asia. Nature, 373: 55–58

Bohaty S M, Zachos J C, Florindo F, Delaney M L. 2009. Coupled greenhouse warming and deep-sea acidification in the middle Eocene. Paleoceanography, 24: 1–16

Bosboom R E, Abels H A, Hoorn C, van den Berg B C J, Guo Z J, Dupont-Nivet G. 2014a. Aridification in continental Asia after the Middle Eocene climatic optimum (MECO). Earth Planet Sci Lett, 389: 34–42

Bosboom R E, Dupont-Nivet G, Houben A J P, Brinkhuis H, Villa G, Mandic O, Stoica M, Zachariasse W J, Guo Z J, Li C X, Krijgsman W. 2011. Late Eocene sea retreat from the Tarim basin (west China) and concomitant Asian paleoenvironmental change. Palaeogeogr Palaeoclimatol Palaeoecol, 299: 385–398

Bosboom R, Dupont-Nivet G, Grothe A, Brinkhuis H, Villa G, Mandic O, Stoica M, Kouwenhoven T, Huang W, Yang W, Guo Z J. 2014b. Timing, cause and impact of the late Eocene stepwise sea retreat from the Tarim Basin (west China). Palaeogeogr Palaeoclimatol Palaeoecol, 403: 101–118

Bougeois L, Dupont-Nivet G, de Rafélis M, Tindall J C, Proust J N, Reichart G J, de Nooijer L J, Guo Z, Ormukov C. 2018. Asian monsoons and aridification response to Paleogene sea retreat and Neogene westerly shielding indicated by seasonality in Paratethys oysters. Earth Planet Sci Lett, 485: 99–110

Burtman V S. 2000. Cenozoic crustal shortening between the Pamir and Tien Shan and a reconstruction of the Pamir-Tien Shan transition zone for the Cretaceous and Palaeogene. Tectonophysics, 319: 69–92

Cai F, Ding L, Yue Y. 2011. Provenance analysis of upper Cretaceous strata in the Tethys Himalaya, southern Tibet: Implications for timing of India-Asia collision. Earth Planet Sci Lett, 305: 195–206

Caves J K, Winnick M J, Graham S A, Sjostrom D J, Mulch A, Chamberlain C P. 2015. Role of the westerlies in Central Asia climate over the Cenozoic. Earth Planet Sci Lett, 428: 33–43

Chamley H. 1989. Clay Sedimentology. New York: Spring-Verlag Berlin Heidelberg

Chen C F. 2009. Cenozoic pollen records and Palaoenvironmental evolution in Xining Basin, Northeastern Tibetan Plateau. Masteral Dissertation. China: Lanzhou University

Dai S, Fang X M, Dupont-Niver G, Song C H, Gao J P, Krijgsman W, Langereis C, Zhang W L. 2006. Magnetostratigraphy of Cenozoic sediments from the Xining Basin: Tectonic implications for the northeastern Tibetan Plateau. J Geophys Res, 111: B11102

Deng Y P, Hong H L, Yin k, Xu Y M, Du J, Zhang K X. 2010. Clay mineralogy and its palaeoclimatic indicator of the Late Paleocene to Early Oligocene Sediments in Yongdeng Lanzhou Basin (in Chinese with English abstract). Geoscience, 24: 793–800

Ding L, Kapp P, Wan X. 2005. Paleocene-Eocene record of ophiolite obduction and initial India-Asia collision, south central Tibet. Tectonics, 24: TC3001

Ding Z L, Xiong S F, Sun J M, Yang S L, Gu Z Y, Liu T S. 1999. Pedostratigraphy and paleomagnetism of a ~7.0 Ma eolian loess-red clay sequence at Lingtai, Loess Plateau, north-central China and the implications for paleomonsoon evolution. Palaeogeogr Palaeoclimatol Palaeoecol, 152: 49–66

Dupont-Nivet G, Hoorn C, Konert M. 2008. Tibetan uplift prior to the Eocene-Oligocene climate transition: Evidence from pollen analysis of the Xining Basin. Geology, 36: 987–990

Dupont-Nivet G, Krijgsman W, Langereis C G, Abels H A, Dai S, Fang X. 2007. Tibetan plateau aridification linked to global cooling at the Eocene-Oligocene transition. Nature, 445: 635–638

Edgar K M, Wilson P A, Sexton P F, Gibbs S J, Roberts A P, Norris R D. 2010. New biostratigraphic, magnetostratigraphic and isotopic insights into the Middle Eocene climatic optimum in low latitudes. Palaeogeogr Palaeoclimatol Palaeoecol, 297: 670–682

Eldrett J S, Greenwood D R, Harding I C, Huber M. 2009. Increased seasonality through the Eocene to Oligocene transition in northern high latitudes. Nature, 459: 969–973

Fang X M, Zan J B, Appel E, Lu Y, Song C H, Dai S, Tuo S B. 2015. An Eocene-Miocene continuous high resolution rock magnetic record from the sediments in the Xining Basin, NW China: Indication for Cenozoic persistent drying driven by global cooling and Tibetan Plateau uplift. Geophys J Int, 201: 78–89

Guo Z T, Ruddiman W F, Hao Q Z, Wu H B, Qiao Y S, Zhu R X, Peng S Z, Wei J J, Yuan B Y, Liu T S. 2002. Onset of Asian desertification by 22 Myr ago inferred from loess deposits in China. Nature, 416: 159–163

Guo Z T, Sun B, Zhang Z S, Peng S Z, Xiao G Q, Ge J Y, Hao Q Z, Qiao Y S, Liang M Y, Liu J F, Yin Q Z, Wei J J. 2008. A major reorganization of Asian climate regime by the early Miocene. Clim Past, 4: 153–174

Gylesjö S, Arnold E. 2006. Clay mineralogy of a red clay-loess sequence from Lingtai, the Chinese Loess Plateau. Glob Planet Change, 51: 181–194

Hetzel R, Dunkl I, Haider V, Strobl M, von Eynatten H, Ding L, Frei D. 2011. Peneplain formation in southern Tibet predates the India-Asia collision and plateau uplift. Geology, 39: 983–986

Hong H L, Zhang K X, Li Z H. 2010. Climatic and tectonic uplift evolution since ~7 Ma in Gyirong basin, southwestern Tibet plateau: Clay mineral evidence. Int J Earth Sci-Geol Rundsch, 99: 1305–1315
Hoorn C, Straathof J, Abels H A, Xu Y, Utescher T, Dupont-Nivet G. 2012. A late Eocene palynological record of climate change and Tibetan Plateau uplift (Xining Basin, China). Palaeogeogr Palaeoclimatol Palaeoecol, 344-345: 16–38
Hren M T, Sheldon N D, Grimes S T, Collinson M E, Hooker J J, Bugler M, Lohmann K C. 2013. Terrestrial cooling in Northern Europe during the Eocene-Oligocene transition. Proc Natl Acad Sci USA, 110: 7562–7567
Hu B, Zhang C X, Guo Z T. 2016. A new method of clay mineral extraction from gypsum layer and its application in paleoclimate reconstruction (in Chinese with English abstract). Quat Sci, 34: 926–934
Kent-Corson M L, Ritts B D, Zhuang G, Bovet P M, Graham S A, Page Chamberlain C. 2009. Stable isotopic constraints on the tectonic, topographic, and climatic evolution of the northern margin of the Tibetan Plateau. Earth Planet Sci Lett, 282: 158–166
Kraatz B P, Geisler J H. 2010. Eocene-Oligocene transition in Central Asia and its effects on mammalian evolution. Geology, 38: 111–114
Lear C H, Bailey T R, Pearson P N, Coxall H K, Rosenthal Y. 2008. Cooling and ice growth across the Eocene-Oligocene transition. Geology, 36: 251–254
Lear C H, Elderfield H, Wilson P A. 2000. Cenozoic deep-sea temperatures and global ice volumes from Mg/Ca in benthic foraminiferal calcite. Science, 287: 269–272
Lippert P C, van Hinsbergen D J J, Dupont-Nivet G. 2014. Early Cretaceous to present latitude of the central proto-Tibetan Plateau: A paleomagnetic synthesis with implications for Cenozoic tectonics, paleogeography, and climate of Asia. Geol Soc Am Spec Pap, 507: 1–23
Liu T S, Guo Z T. 1997. Geological environment in China and global change. In: An Z S, ed. Selected Works of Liu Tungsheng. Beijing: Science Press. 192–202
Liu T S. 1985. Loess and Environment (in Chinese). Beijing: Science Press
Long L Q, Fang X M, Miao Y F, Bai Y, Wang Y L. 2011. Northern Tibetan Plateau cooling and aridification linked to Cenozoic global cooling: Evidence from n-alkane distributions of Paleogene sedimentary sequences in the Xining Basin. Chin Sci Bull, 56: 1221–1231
Miao Y F, Fang X M, Song Z C, Wu F L, Han W X, Dai S, Song C H. 2008. Late Eocene pollen records and palaeoenvironmental changes in northern Tibetan Plateau. Sci China Ser D-Earth Sci, 51: 1089–1098
Miao Y, Wu F, Chang H, Fang X, Deng T, Sun J, Jin C. 2016. A Late-Eocene palynological record from the Hoh Xil Basin, northern Tibetan Plateau, and its implications for stratigraphic age, paleoclimate and paleoelevation. Gondwana Res, 31: 241–252
Moore D M, Reynolds J. 1989. X-Ray Diffraction and the Identification and Analysis of Clay Minerals. New York: Oxford University Press
Najman Y, Appel E, Boudagher-Fadel M, Bown P, Carter A, Garzanti E, Godin L, Han J, Liebke U, Oliver G, Parrish R, Vezzoli G. 2010. Timing of India-Asia collision: Geological, biostratigraphic, and palaeomagnetic constraints. J Geophys Res, 115: B12416
Patzelt A, Li H, Wang J, Appel E. 1996. Palaeomagnetism of Cretaceous to Tertiary sediments from southern Tibet: Evidence for the extent of the northern margin of India prior to the collision with Eurasia. Tectonophysics, 259: 259–284
Pearson P N, Foster G L, Wade B S. 2009. Atmospheric carbon dioxide through the Eocene-Oligocene climate transition. Nature, 461: 1110–1113
Pei J L, Sun Z M, Wang X S, Zhao Y, Ge X H, Guo X Z, Li H B, Si J L. 2009. Evidence for Tibetan plateau uplift in Qaidam basin before Eocene-Oligocene boundary and its climatic implications. J Earth Sci, 20: 430–437
Petschick R. 2000. MacDiff 4.2.2: A software of calculating concentration of minerals for XRD data. Online: http://servermac.geologie.un-frankfurt.de/ Rainer.html
Prell W L, Kutzbach J E. 1992. Sensitivity of the indian monsoon to forcing parameters and implications for its evolution. Nature, 360: 647–652
Qiang X, An Z, Song Y, Chang H, Sun Y, Liu W, Ao H, Dong J, Fu C, Wu F, Lu F, Cai Y, Zhou W, Cao J, Xu X, Ai L. 2011. New eolian red clay sequence on the western Chinese Loess Plateau linked to onset of Asian desertification about 25 Ma ago. Sci China Earth Sci, 54: 136–144
Qinghai Bureau of Geology and Mineral Resources. 1985. Geologic Maps of the Duoba, Gaodian, Tianjiazai, and Xining Regions, 4 Sheets, with Regional Geologic Report (1:50000 Scale). Beijing: Geol Publ House. 199
Robert C, Kennett J P. 1994. Antarctic subtropical humid episode at the Paleocene-Eocene boundary: Clay-mineral evidence. Geology, 22: 211–214
Rohrmann A, Kapp P, Carrapa B, Reiners P W, Guynn J, Ding L, Heizler M. 2012. Thermochronologic evidence for plateau formation in central Tibet by 45 Ma. Geology, 40: 187–190
Rowley D B. 1996. Age of initiation of collision between India and Asia: A review of stratigraphic data. Earth Planet Sci Lett, 145: 1–13
Rowley D B, Currie B S. 2006. Palaeo-altimetry of the late Eocene to Miocene Lunpola basin, central Tibet. Nature, 439: 677–681
Ruddiman W F, Kutzbach J E. 1989. Forcing of late Cenozoic northern hemisphere climate by plateau uplift in southern Asia and the American West. J Geophys Res, 94: 18409
Sayem A S M, Guo Z, Wu H, Zhang C, Yang F, Xiao G, He Z. 2018. Sedimentary and geochemical evidence of Eocene climate change in the Xining Basin, northeastern Tibetan Plateau. Sci China Earth Sci, 61: 1292–1305
Shi N. 1996. Development of spruce and fir in North China during the Pliocene and the Early Plestocene: Palaeoclimatic implication. Quat Sci, 4: 319–328
Singer A. 1984. The paleoclimatic interpretation of clay minerals in sediments—A review. Earth-Sci Rev, 21: 251–293
Song B W, Zhang K X, Lu J F, Wang C W, Xu Y D. 2013. The middle Eocene to early Miocene integrated sedimentary record in the Qaidam Basin and its implications for paleoclimate and early Tibetan Plateau uplift. Can J Earth Sci, 50: 183–196
Sun X J, Wang P X. 2005. How old is the Asian monsoon system?—Palaeobotanical records from China. Palaeogeogr Palaeoclimatol Palaeoecol, 222: 181–222
Tang T, Xue Y, Yu C. 1992. Characteristics and Sedimentary Environments of the Late Cretaceous to Early Tertiary Marine Strata in the Western Tarim, China. Beijin: Science Press
Velde B. 1995. Origin and Mineralogy of Clays. Paris: Springer-Verlag Berlin and Heidelberg. 207–210
Vonhof H B, Smit J, Brinkhuis H, Montanari A, Nederbragt A J. 2000. Global cooling accelerated by early late Eocene impacts? Geology, 28: 687
Wang C S, Li X H, Hu X, Jansa L F. 2002. Latest marine horizon north of Qomolangma (Mt Everest): Implications for closure of Tethys seaway and collision tectonics. Terra Nova, 14: 114–120
Wang C S, Zhao X X, Liu Z F, Lippert P C, Graham S A, Coe R S, Yi H S, Zhu L D, Liu S, Li Y L. 2008. Constraints on the early uplift history of the Tibetan Plateau. Proc Natl Acad Sci USA, 105: 4987–4992
Wang C W, Hong H L, Li Z H, Yin K, Xie J, Liang G J, Song B W, Song E P, Zhang K X. 2013. The Eocene-Oligocene climate transition in the Tarim Basin, Northwest China: Evidence from clay mineralogy. Appl Clay Sci, 74: 10–19
Wang C W, Hong H L, Song B W, Yin K, Li Z H, Zhang K X, Ji J L. 2011. The early-Eocene climate optimum (EECO) event in the Qaidam basin, northwest China: Clay evidence. Clay miner, 46: 649–661
Xiao G Q. 2009. Magnetostratigraphy and Sedimentary Evolution of the Late Eocene–early Miocene Deposits in the Xining Basin, Northwestern China. Doctoral Dissertation. China: Institute of Earth Environment, Graduate School, CAS
Xiao G Q, Abels H A, Yao Z Q, Dupont-Nivet G, Hilgen F J. 2010. Asian aridification linked to the first step of the Eocene-Oligocene climate Transition (EOT) in obliquity-dominated terrestrial records (Xining Basin, China). Clim Past, 6: 501–513
Xu Q, Ding L, Zhang L, Cai F, Lai Q, Yang D, Liu-Zeng J. 2013. Paleo-

gene high elevations in the Qiangtang Terrane, central Tibetan Plateau. Earth Planet Sci Lett, 362: 31–42
Yi Z, Huang B, Chen J, Chen L, Wang H. 2011. Paleomagnetism of early Paleogene marine sediments in southern Tibet, China: Implications to onset of the India-Asia collision and size of Greater India. Earth Planet Sci Lett, 9: 153–165
Yue L, Heller F, Qiu Z, Zhang L, Xie G, Qiu Z, Zhang Y. 2001. Magnetostratigraphy and pavleo-environmental record of Tertiary deposits of Lanzhou Basin. Chin Sci Bull, 46: 770–773
Zachos J C, Dickens G R, Zeebe R E. 2008. An early Cenozoic perspective on greenhouse warming and carbon-cycle dynamics. Nature, 451: 279–283
Zachos J C, Röhl U, Schellenberg S A, Sluijs A, Hodell D A, Kelly D C, Thomas E, Nicolo M, Raffi I, Lourens L J, McCarren H, Kroon D. 2005. Rapid acidification of the ocean during the Paleocene-Eocene thermal maximum. Science, 308: 1611–1615
Zachos J C, Wara M W, Bohaty S, Delaney M L, Petrizzo M R, Brill A, Bralower T J, Premoli-Silva I. 2003. A transient rise in tropical sea surface temperature during the Paleocene-Eocene thermal maximum. Science, 302: 1551–1554
Zachos J, Pagani M, Sloan L, Thomas E, Billups K. 2001. Trends, rhythms, and aberrations in global climate 65 Ma to present. Science, 292: 686–693
Zanazzi A, Kohn M J, MacFadden B J, Terry D O. 2007. Large temperature drop across the Eocene–Oligocene transition in central North America. Nature, 445: 639–642
Zhang C X, Guo Z T. 2014. Clay mineral changes across the Eocene-Oligocene transition in the sedimentary sequence at Xining occurred prior to global cooling. Palaeogeogr Palaeoclimatol Palaeoecol, 411: 18–29
Zhang C X, Xiao G Q, Guo Z T, Wu H B, Hao Q Z. 2015. Evidence of late early Miocene aridification intensification in the Xining Basin caused by the northeastern Tibetan Plateau uplift. Glob Planet Change, 128: 31–46
Zhang J, Wang Y N, Zhang B H, Zhang Y P. 2016. Tectonics of the Xining Basin in NW China and its implications for the evolution of the NE Qinghai-Tibetan Plateau. Basin Res, 28: 159–182
Zhang Y, Kong S C, Yan S, Yang Z J, Ni J. The variation of forest line in the north slope of Tian Shan Mountain in the Holocene and its palaeoenvironment feature. Chin Sci Bull, 2006, 51: 1450–1458
Zhang Z S, Flatøy F, Wang H J, Bethke I, Bentsen M, Guo Z T. 2012. Early Eocene Asian climate dominated by desert and steppe with limited monsoons. J Asian Earth Sci, 44: 24–35
Zhu B, Kidd W S F, Rowley D B, Currie B S, Shafique N. 2005. Age of initiation of the India-Asia collision in the East-Central Himalaya. J Geol, 113: 265–285

(Responsible editor: Huayu LU)